SnO 2 films elaborated by radio frequency (RF)magnetron sputtering as a potential TCOs alternative for organic solar cells

Wissal Belayachi, Gérald Ferblantier, Thomas Fix, Guy Schmerber, Jean-Luc Rehspringer, Thomas Heiser, Abdelilah Slaoui, Mohammed Abd-Lefdil, Aziz Dinia

SnO_2 films elaborated by radio frequency (RF)-magnetron sputtering as a potential TCOs alternative for organic solar cells

Wissal Belayachi [†, §,], Gérald Ferblantier [‡], Thomas Fix [‡], Guy Schmerber [†], Jean-Luc Rehspringer [†], Thomas Heiser [‡], Abdelilah Slaoui [‡], Mohammed Abd-Lefdil [§] and Aziz Dinia [†].*

† Université de Strasbourg, CNRS, Institut de Physique et Chimie des Matériaux de Strasbourg, UMR 7504, 23 rue du Loess, F-67000 Strasbourg, France.

§ Mohammed V University in Rabat, Faculty of Sciences, MANAPSE, B.P. 1014, 10000 Rabat, Morocco.

‡ ICube laboratory (Université de Strasbourg and CNRS), 23 rue du Loess, BP 20 CR, F-67037 Strasbourg Cedex 2, France

KEYWORDS: Organic solar cells; Transparent conducting oxide, Tin oxide; Reactive magnetron sputtering; Thin films; Bulk heterojunction.

ABSTRACT

Transparent conducting oxides (TCOs) are crucial component of solar cells. Tin doped indium oxide (ITO) is the most employed TCO, but the scarcity and high price of indium induce a search for lower cost TCOs with equivalent properties as substitute. Tin dioxide (SnO_2) films have many advantages, such as rich sources of material, low prices, and non-toxicity. SnO_2 films present a high visible light transmittance, near-infrared light reflectivity, and excellent electrical properties. They also have a higher chemical and mechanical stability compared to ITO. The aim of this work is to elaborate SnO_2 films by RF-magnetron sputtering in order to use them as electrodes for Organic Solar Cells (OSCs). The SnO_2 films were deposited on glass, SiO_2 and quartz substrates in a mixed environment of Ar and O_2. XRD measurements show that the as-deposited SnO_2 films are polycrystalline with cassiterite tetragonal structure. SEM analysis showed that the films are homogeneous, continuous, and nanostructured. The electrical resistivity and average optical transmittance of the samples are about 10^{-3} Ω.cm and over 80%, respectively. The estimated optical band gap (E_g) is around 4.0 eV while the work function of the films is around 5.0 eV. The SnO_2 films are used as electrodes for inverted OSCs, using poly(3-hexylthiophene-2,5-diyl): [6,6]-phenyl-C60-butryric acid methyl ester (P3HT:$PC_{60}BM$) as active layer. The device's open circuit voltage (V_{OC}) and short circuit current density (J_{SC}) are similar to those obtained for the inverted OSCs employing ITO as the same electrode. Even if the achieved power conversion efficiency is lower compared to the value for the reference OSC with an ITO electrode, these results are promising and place SnO_2 TCO as a potential candidate to replace ITO.

1. INTRODUCTION

Transparent conductive oxides (TCOs) are extensively used in modern semiconductor devices such as liquid crystal displays (LCD)[1,2], organic light emitting diodes (OLEDs)[3], touch-sensitive screens[4], photovoltaic devices[5,6], gas sensors[7,8], and smart windows[9] due to their high electrical conductivity and high optical transmission. Tin doped indium oxide (ITO) thin films are widely used as TCOs because of their low resistivity (in the range of 10^{-4} Ω.cm), high light transmittance in the visible region (around 90%) and multitude of wide-area deposition techniques[2]. However, indium is scarce and in high demand, making it an expensive source material[10].

Tin dioxide (SnO_2) has received significant attention as a viable replacement for ITO due to its attractive properties. SnO_2 is by nature an n-type semiconductor with a wide and direct band gap, of 3.6 up to 4.0 eV at room temperature[9,11], and a high work function of about 5.1 eV[11]. SnO_2 is highly transparent in the visible region, chemically stable in some acidic and basic solutions[12], thermally stable in oxidizing environments at high temperature, and mechanically hard[10]. SnO_2 thin films are prepared through different deposition techniques such as DC/RF magnetron sputtering[10,13–19], pulsed laser deposition[20,21], thermal evaporation[22,23], sol-gel[24–26], spray pyrolysis[27,28], chemical vapor deposition[8,29,30], and hydrothermal process[31,32].

RF-magnetron sputtering has various advantages such as good adhesion to substrates, homogeneity of deposited thin films, good reproducibility, and the possibility to extend the deposition technique to industrial scale[33]. Therefore, it was selected as deposition technique for this study. The structural, optical, and electrical properties of SnO_2 thin films deposited by RF-magnetron sputtering have been investigated for a substrate temperature ranging from 100 up to 400°C and for an Ar/O_2 gas ratio of 8/3. The film with the lowest electrical resistivity was then employed as electrode for an inverted Organic Solar Cell (OSC), and the photovoltaic properties of the solar cell were studied.

2. Experimental section

2.1.Materials

The following chemicals were purchased: polyethylenimine (80% ethoxylated, 37 wt. % in H_2O), acetone (CH_3COCH_3, ACS reagent, ≥99.5%), anhydrous 1,2-Dichlorobenzene ($C_6H_4Cl_2$, 99%), and Hellmanex™ III from Sigma-Aldrich; [6,6]-phenyl-C60-butryric acid methyl ester ([60]PCBM, 99.5%) from Solenne BV; poly(3-hexylthiophene-2,5-diyl) (P3HT) from Solaris Chem; molybdenum oxide (MoO_3, 99.95%) from Neyco; silver pellets (Ag, 99.99%) from RD Mathis Company; ethanol absolute (C_2H_5OH, 100%), hydrochloric acid (HCl, 37%) and 2-propanol (IPA) ($(CH_3)_2CHOH$, 100%) from VWR Chemicals; zinc powder (metals basis, -140+325 mesh, 99.9%) from Alfa Aesar; chromium powder (metals basis, ≤ 5 µm, 99.8%) from CERAC; AZ 4533 positive photoresist and AZ 726 metal ion free (MIF) developer from Clariant. All the chemicals were directly used without further purification.

2.2.SnO_2 thin film and solar cell fabrication

2.2.1. SnO_2 thin films preparation

In order to characterize the active layer, SnO_2 thin films were deposited on oriented SiO_2 (100), polished soda lime glass and synthetic quartz substrates. Prior to the deposition the substrates were ultrasonically cleaned with deionized water with Hellmanex™ III, deionized water, acetone, and 2-propanol for 15 min each at 45°C and dried under N_2 gas flow. The thin films were deposited by (RF)-magnetron sputtering using high purity (99.95%) tin (Sn) target from AJA Int. High purity argon (Ar) and oxygen (O_2) were introduced into the sputtering chamber through flowmeters. The Ar and O_2 flows are kept 8 sccm and 3 sccm, respectively. These gas flows were chosen based on the results obtained of the study of the effect of Ar/O_2 ratio on the films resistivity (Support A).

The substrates were placed on a substrate holder with heating block. The working pressure was kept at 3.4×10^{-3} mbar with a source-substrate distance of 25 cm and sputtering power of 50 W. The deposition rate was 3 nm/min. The substrate temperatures were ranging from 100 up to 400°C and an increment of 100°C is made between each treatment.

2.2.2. Device fabrication

The SnO_2 thin films deposited on glass substrates (2 cm × 2 cm) were patterned by optical photolithography and wet etching (Supplementary B). The thin films were treated in UV Ozone for 30 min to remove any organic residue.

ITO coated glass substrates (2 cm × 2 cm) were purchased from Lumtec (Taiwan). They were characterized as a mean of comparison and employed for the elaboration of a reference device. Prior to the deposition the ITO substrates were ultrasonically cleaned with deionized water with Hellmanex™ III, deionized water, acetone, and 2-propanol for 15 min each at 45°C and dried under N_2 gas flow. They were also treated in UV Ozone for 30 min to remove any organic residue.

The electron transport layer was prepared by spin-coating polyethylenimine (PEIE) solution (0.4% in mass of PEIE in IPA) onto the SnO_2 film at 5000 rpm for 60s. The layer is then annealed at 100 °C for 10 min in N_2 glove box. The P3HT:PC_{60}BM solution (donor/acceptor ratio 1:0.6) was prepared by dissolving the precursors in 1,2-Dichlorobenzene (ODCB). The solution was heated and stirred on a hot plate at 60°C for at least 24 h. The active layer was spin-coated from the solution on the substrate in N_2 glove box at 500 rpm for 20 s then 1200 rpm for 90 s. The layer is then annealed at 150 °C for 15 min. A 7 nm-thick MoO_3 layer, or hole transporting layer, and a 120 nm-thick Ag electrode were deposited in a single run by thermal evaporation, under high vacuum (5×10^{-6} to 2×10^{-7} Torr). A metal shadow mask is used in proximity of the substrate to

delimit the areas to coat with the organic layer and the metal electrode. The MoO_3 and Ag layers were deposited at a rate of 0.5 Å/s and 3.5 Å/s, respectively, as measured by a quartz microbalance.

2.3.Characterization

X-ray powder diffraction (XRD) patterns were collected using a Rigaku Smartlab X-ray diffractometer with $CuK_{\alpha 1}$ radiation (λ = 1.54056 Å) operated at 45 kV and 200 mA, in the 2θ range of 15 – 70° with a step size of 0.06° and with a scanning rate (2θ) of 0.3°/min. Phase analysis was conducted using the Eva XRD software.

Scanning electron microscopy (SEM) was performed using a field emission scanning electron microscope. Surface SEM images were recorded using a Jeol 6700 F and the cross-section SEM images using a Zeiss Gemini 500. The SEM scans were recorded for 5K, 50K and 80K magnification at 5 kV applied voltage for Zeiss and 7kV applied voltage for Jeol.

UV-Vis spectroscopy was carried out using a Perkin-Elmer Lambda 950 spectrophotometer over the spectral range 300 – 1000 nm. An integrating sphere was used to collect both, specular and diffuse transmittance to reduce the effect of light scattering originated from refraction and reflection.

The thickness of the films was measured using a Veeco Dektak 150 surface profilometer. To produce a step in the films, Kapton tape was applied to a small area of the SiO_2 substrate before the deposition. The tape was easily removed with acetone after the deposition to reveal a step in the film down to the substrate.

Electrical characteristics were acquired in the dark using Hall measuring equipment in the Van-der Pauw's geometry, with an Ecopia HMS-5000 system, at room temperature. A direct current of

1 mA and a magnetic field of 0.55 T were applied. The measurements were repeated 5 times to ensure reproducibility and the results were averaged to compensate deviations.

The films work function was measured using a Single-Point Kelvin Probe system (KP020) from KP Technology in ambient air and at room temperature.

The current density-voltage (J-V) characteristics were recorded with a Keithley 2400 source meter and a Sun 3000 Solar Simulator with the light intensity of 100 mW/cm^2 under AM 1.5 G solar light. The active area of the measured devices was 0.12 cm^2, and a mask was used during the measurements.

3. RESULTS AND DISCUSSION

3.1.Structure and morphology

3.1.1. X-Ray Diffraction

The XRD patterns of the SnO_2 films deposited at different substrate temperatures T_S are shown in Figure 1. All the observed diffraction peaks can be indexed according to the cassiterite tetragonal structure of SnO_2 (JCPDS card n° 01-071-5323). A peak characteristic of the SnO_x phase is observed at approximately 24.42° (2θ). An increase in sharpness and intensity of the XRD peaks can be observed with the increase of the substrate temperature.

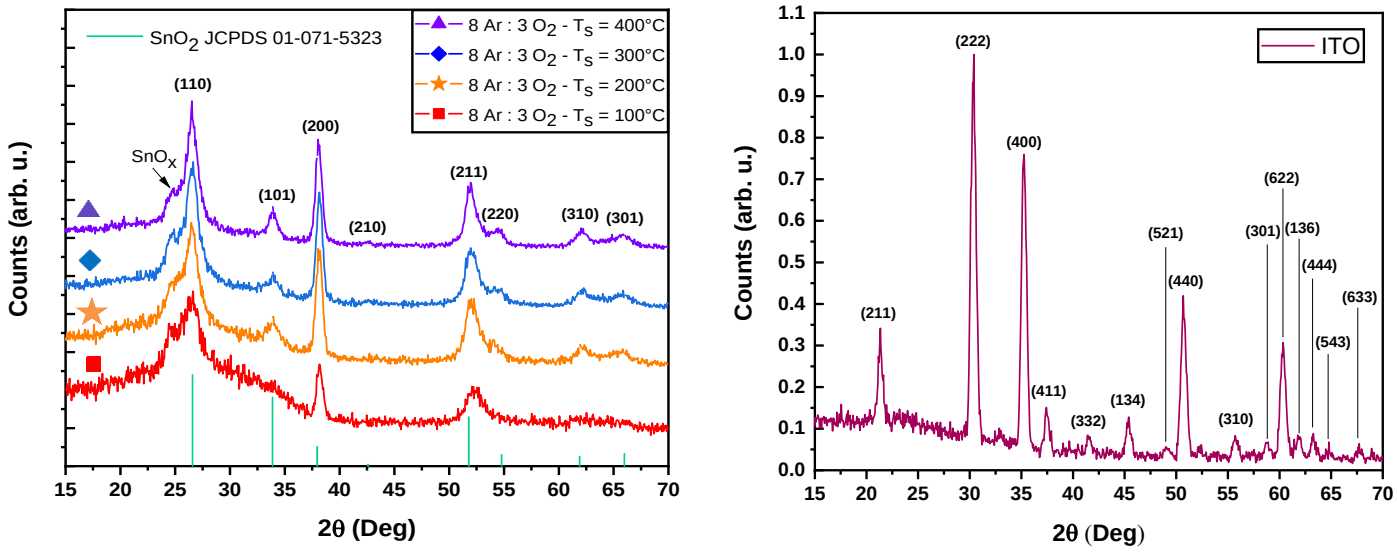

146 **Figure 1.** X-ray diffraction pattern of a) SnO_2 films deposited on glass substrates with different
147 substrate temperatures and, b) commercial ITO. The patterns have been translated vertically for
148 better viewing purposes.

149 The tetragonal structure lattice parameters *a*, *b* and *c* are defined as follows:

$$\frac{1}{d^2} = \frac{h^2 + k^2}{a^2} + \frac{l^2}{c^2}\,, \tag{1}$$

150 where *d* is the lattice spacing between two different crystallographic planes, and *h*, *k*, *l* the miller
151 indexes of the reflection plane. From the results presented in Table 1 we can see that *a* and *c* are
152 rather stable when increasing the substrate temperature T_S. Overall the lattice parameters *a, b* and
153 *c* are slightly lower with respect to the standard values $a=b=4.737$ Å, $c=3.185$ Å present in the
154 literature[9] (JCPDS card n° 01-071-5323). The lower lattice parameters and the presence of a SnO_x
155 phase show that the SnO_2 films are probably non-stoichiometric.

156 The crystallite size *D* of the SnO_2 films is estimated using the Scherrer formula[34] (Equation 2):

$$D = \frac{K\lambda}{\beta\, cos(\theta)}\,, \tag{2}$$

where D is the average crystallite size perpendicular to the reflecting planes, λ is the X-ray light wavelength, β is the width of the X-ray peak on the 2θ axis, normally measured as full width at half maximum (FWHM), θ is the Bragg angle, and K is the so-called Scherrer constant. K depends on the crystallite shape and the size distribution, indices of the diffraction line and taken equal to 0.9 here. The calculated values of D (Table 1) represent estimates (discussion on the accuracy of Equation (2) can be found in the literature[35]). D slightly rises with the substrate temperature as it was previously reported by Bansal et al and by Kim et al[11,33].

The amount of defects in the SnO_2 films can be determined by estimating the dislocation density δ which is defined using the approach of Williamson and Smallman[36] (Equation 3):

$$\delta = \frac{1}{D^2}, \tag{3}$$

where D is the average crystallite size. As the substrate temperature increases δ decreases indicating the reduction of the defects generated in the SnO_2 samples. To our knowledge no studies report on the effect of substrate temperature on the dislocation density of undoped SnO_2 films elaborated by (RF)-magnetron sputtering. In comparison, the commercial ITO presents a dislocation density δ (Table 1) lower than all SnO_2 films which is explained by the ITO's higher average crystallite size D. Therefore, the commercial ITO presumably presents fewer defects than all SnO_2 films.

In conclusion, the XRD analysis shows that a substrate temperature of 400°C gives the best crystallinity.

Table 1. Unit cell parameters *a, b* and *c*, unit cell volume *V*, crystallite size *D*, and dislocation density δ of the SnO_2 films and commercial ITO.

Sample	$a=b$ (Å)	c (Å)	V (Å^3)	D (nm)	δ (10^3 lines/μm^2)
T_S = 100°C	4.614 ± 0.011	3.063 ± 0.016	65.23 ± 0.37	11.3 ± 4.8	7.95 ± 0.48
T_S = 200°C	4.629 ± 0.023	3.110 ± 0.050	66.65 ± 0.86	11.7 ± 4.7	7.29 ± 0.44
T_S = 300°C	4.611 ± 0.010	3.140 ± 0.041	66.76 ± 0.84	12.3 ± 4.2	6.67 ± 0.33
T_S = 400°C	4.628 ± 0.013	3.110 ± 0.035	66.61 ± 0.67	12.6 ± 2.7	6.28 ± 0.25
ITO	10.173 ± 0.001	10.173 ± 0.001	1052.80 ± 0.31	42.6 ± 1.3	5.51 ± 0.33

3.1.2. SEM characterization

The SnO_2 films obtained were slightly yellowish, very clear and transparent, with smooth mirror-like surface characteristic to tin dioxide[37]. The surface and cross-section SEM images of the SnO_2 films deposited at different substrate temperatures are given in Figure 2. As for the surface, because the grains of the films are small-sized, only some blurred SEM images can be obtained. The SEM images show that as predicted by the XRD analysis the commercial ITO presents larger sized grains compared to all SnO_2 films.

The SnO_2 films are homogenous in surface. A columnar morphology can be observed with the cross-section images. The thickness of the films is homogenous and continuous throughout the whole length of the films.

190

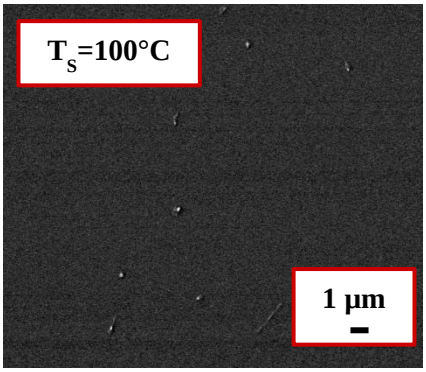
T$_S$=100°C
1 µm

(a)

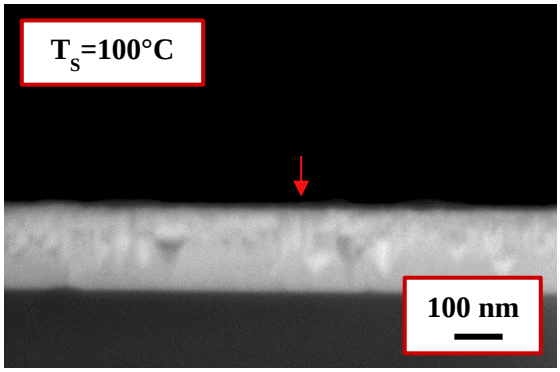
T$_S$=100°C
100 nm

(b)

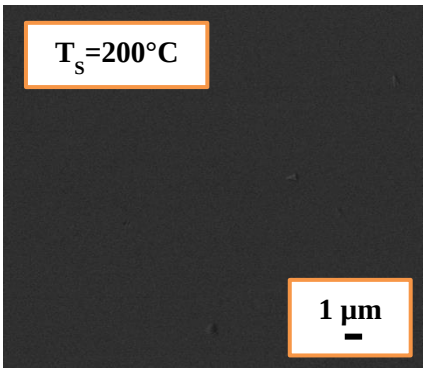
T$_S$=200°C
1 µm

(c)

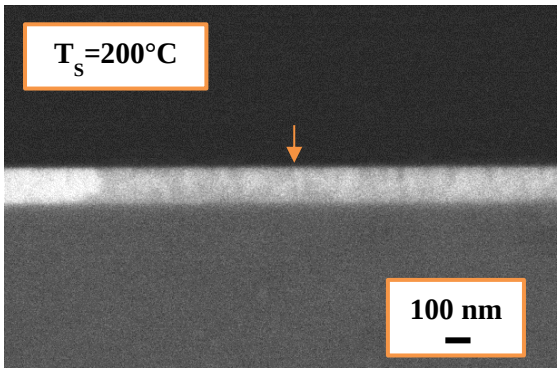
T$_S$=200°C
100 nm

(d)

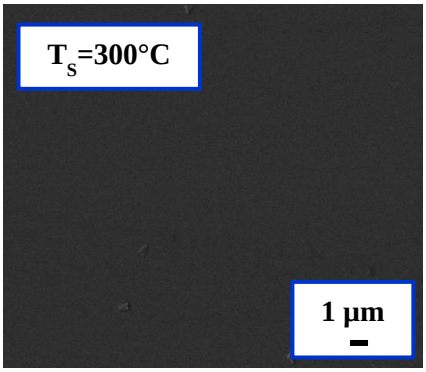
T$_S$=300°C
1 µm

(e)

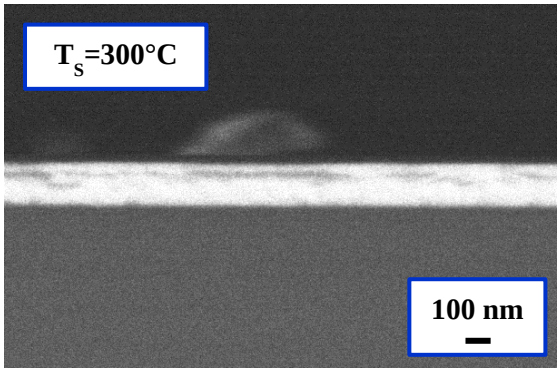
T$_S$=300°C
100 nm

(f)

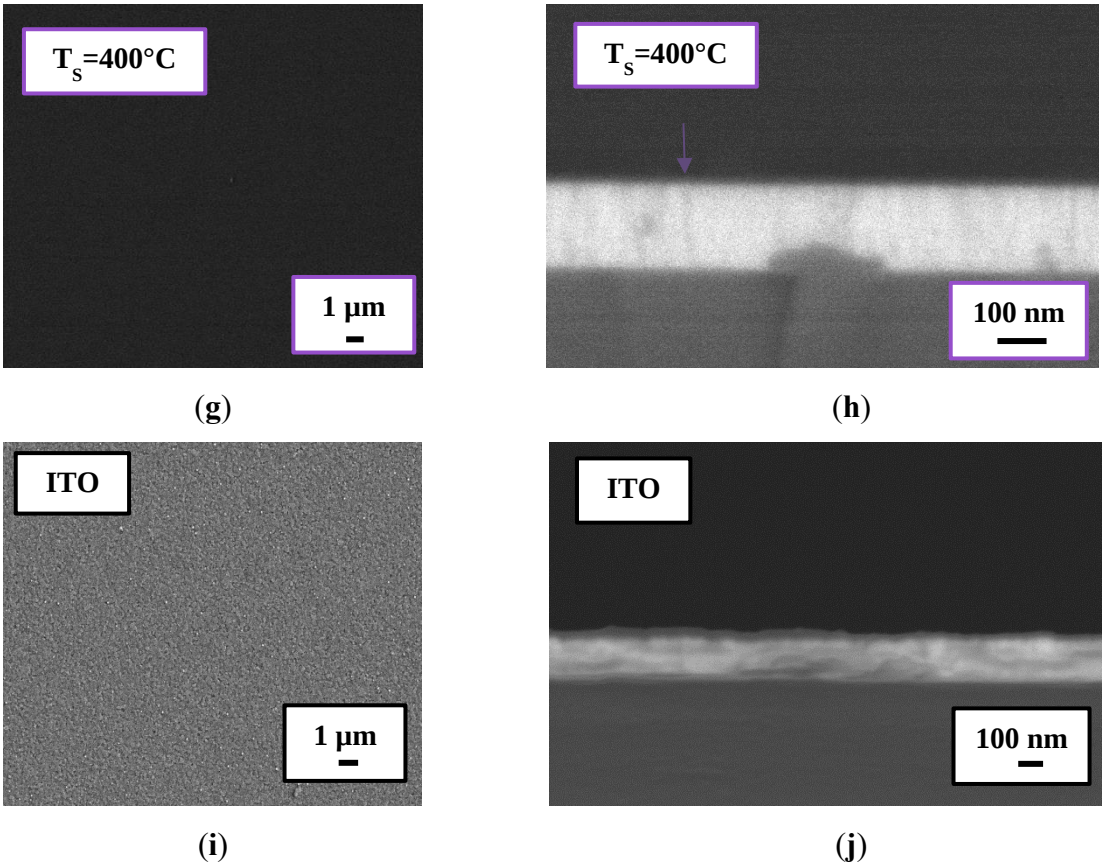

Figure 2. Surface morphology and cross-section SEM images of (a-h) SnO_2 films deposited on glass substrates for different substrate temperatures and, (i-j) commercial ITO.

3.2.Optical properties

Optical characteristics such as the average transmittance in the visible region and the value of the optical band gap are considered to be key features for solar cell applications. The transmittance spectra of the SnO_2 films deposited on glass substrate are displayed in Figure 3a. The average transmittance T_{avg} in the visible range increases from 83.6 up to 84.7% with the substrate temperature (Table 3). As explained by Yang et al[10] a low crystallinity of the films creates inherent defects, which could cause defect scattering. On the other hand, when the crystallinity of the film is improved and the light scattering due to the inherent defect decreases an increase in the average transmittance of the film ensues, as observed for our samples. The effect of substrate temperature

on the average transmittance of the SnO_2 films concurs with the results in the litterature[10,12]. The average transmittance of the prepared SnO_2 films are close to the values reported for undoped SnO_2 films[37–39] and slightly lower than the average transmittance of the commercial ITO (Table 2).

The incident photon energy $h\upsilon$ and the optical bandgap energy E_g are related through Tauc's equation[40] (Equation 4):

$$(\alpha h\upsilon) = A\left(h\upsilon - E_g\right)^{\frac{1}{n}}, \tag{4}$$

where α is the absorption coefficient, h is the Planck constant, $h\upsilon$ is the photon frequency, A a constant and n is related to the type of band transition (2 or 1/2 for direct and indirect transitions, respectively). The absorption coefficient α is calculated through the following relation:

$$\alpha = \frac{1}{t}\ln\left(\frac{1}{T}\right), \tag{5}$$

where T is the optical transmittance and t the thickness of the sample. The thickness t is determined by profilometric analysis for each sample (Table 2). In the assumption of a direct band transition for SnO_2[10,38], E_g was estimated by extrapolating the linear part of Tauc's plots $(\alpha h\upsilon)^2$ vs. $(h\upsilon)$ that intercepts the energy axis (Figure 3b). The estimated optical band gaps are 3.86 ± 0.04 eV for T_S = 100°C, 4.01 ± 0.04 eV for T_S = 200°C, 3.93 ± 0.04 eV for T_S = 300°C and 3.93 ± 0.04 eV for T_S = 400°C. The E_g values obtained are in agreement with the reported values for tetragonal SnO_2[14].

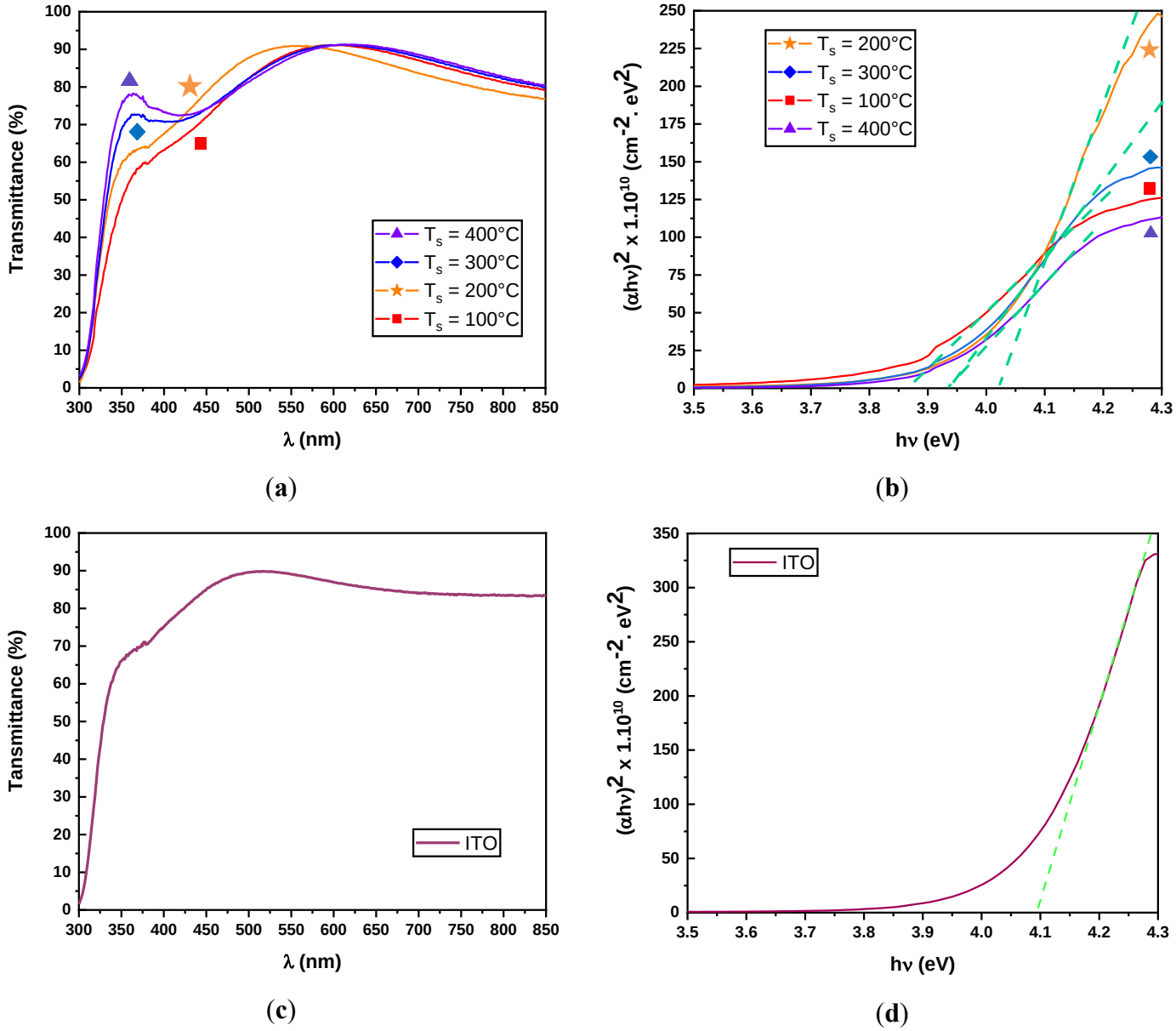

Figure 3. (a,c) UV - Visible transmittance spectrum and (b,d) Tauc's plot of the SnO_2 films for different substrate temperature and commercial ITO.

3.3.Electrical properties

The electrical resistivity ρ is connected to the carrier concentration n and Hall mobility μ by the following relation[39]:

$$\rho = \frac{1}{ne\mu}, \tag{6}$$

The values of ρ, n and μ measured at room temperature for the SnO_2 films grown at various substrate temperatures on quartz are presented in Table 2. The measurements confirm the n-type nature of all prepared SnO_2 films. With the growing substrate temperature, the electrical resistivity increases from 4.45×10^{-3} up to 3.26 Ω.cm while the carrier concentration decreases from 6.78×10^{19} down to 1.21×10^{19} cm^{-3}. The mobility of the free electrons also declines from 20.7 down to 1.58×10^{-1} $cm^2/V.s$. The effect of the substrate temperature on the resistivity of SnO_2 films observed is in agreement with the literature[11,41,42]. The source of carriers for undoped SnO_2 is oxygen vacancies. An increment of temperature leads to a reduction in oxygen vacancies due to chemisorption of oxygen. This phenomenon results in a drop in resistivity but also in carrier concentration observed in our study[11]. It should be noted that a resistivity of order of 10^{-3} Ω.cm is obtained for T_S = 100°C, while it is usually attained for higher substrate temperature[33,41,42].

Compared to commercial ITO (Table 2), the SnO_2 film prepared at T_S = 100°C has a higher electrical resistivity by an order of magnitude. The difference can be explained by the higher carrier concentration n for the commercial ITO by two orders of magnitude.

In addition, a useful tool for comparing the performance of TCOs is the figure of merit Φ_{TC}, as defined by Haacke[43]:

$$\Phi_{TC} = \frac{T^{10}}{R_S}, \tag{7}$$

where T is the optical transmittance and R_S the electrical sheet resistance of the sample. R_S is defined by the electrical resistivity ρ and the thickness d of the sample:

$$R_S = \frac{\rho}{d}, \tag{8}$$

The figure of merit Φ_{TC} being inversely proportional to the electrical resistivity ρ, Φ_{TC} decreases with the temperature. The estimated values of Φ_{TC} (Table 2) show that the SnO_2 film prepared at T_S = 100°C has the potential to be a superior TCO compared to the films elaborated at higher substrate temperatures. The resistivity of ITO being lower than the SnO_2 film prepared at T_S = 100°C the ITO's figure of merit is higher.

The SnO_2 films work function (WF) must match that of the layers of the device employed in. The estimated values are presented in Table 2. For all the samples WF is around 5 eV and in agreement with the literature[11]. The estimated values are similar to the WF of the commercial ITO. Thus, the use of a buffer layer is necessary to improve the energy level alignment with the transport levels of the donor and acceptor employed in the devices.

Table 2. Thickness t, average optical transmittance T_{avg} in the visible range, electrical parameters (n, ρ, μ), figure of merit Φ_{TC} and work function WF values of the SnO_2 films and commercial ITO.

Sample	t (nm)	T_{avg} (%)	n (cm^{-3})	ρ (Ω.cm)	μ ($cm^2/V.s$)	Φ_{TC} (Ω^{-1})	WF (eV)
T_S = 100 °C	155 ± 3	83.6	-6.78×10^{19}	4.45×10^{-3}	20.7	5.77×10^{-4}	5.02
T_S = 200 °C	160 ± 5	84.0	-5.84×10^{19}	2.75×10^{-2}	3.89	1.02×10^{-4}	5.00
T_S = 300 °C	155 ± 5	84.5	-4.22×10^{19}	2.53×10^{-1}	5.85×10^{-1}	1.14×10^{-5}	4.96
T_S = 400 °C	250 ± 10	84.7	-1.21×10^{19}	3.26	1.58×10^{-1}	1.45×10^{-6}	4.99
ITO	165 ±5	90.5	-1.38×10^{21}	1.91×10^{-4}	26.3	1.37×10^{-3}	4.97

3.4.Photovoltaic devices

The requirements for an optimal TCO as replacement for ITO include a high electrical conductivity, a high transmission, and most importantly a proper work function. Therefore, the

SnO_2 film with the lowest electrical resistivity of 4.45×10^{-3} Ω.cm was selected for the elaboration of an inverted OSC, using a blend of poly(3-hexylthiophene-2,5-diyl) (P3HT) and [6,6]-phenyl-C60-butryric acid methyl ester ($PC_{60}BM$) as active layer. A reference device with the same active layer and ITO as electrode is also elaborated. The current density–voltage (J–V) characteristics of the photovoltaic devices are shown in Figure 4 and the photovoltaic parameters are listed in Table 3.

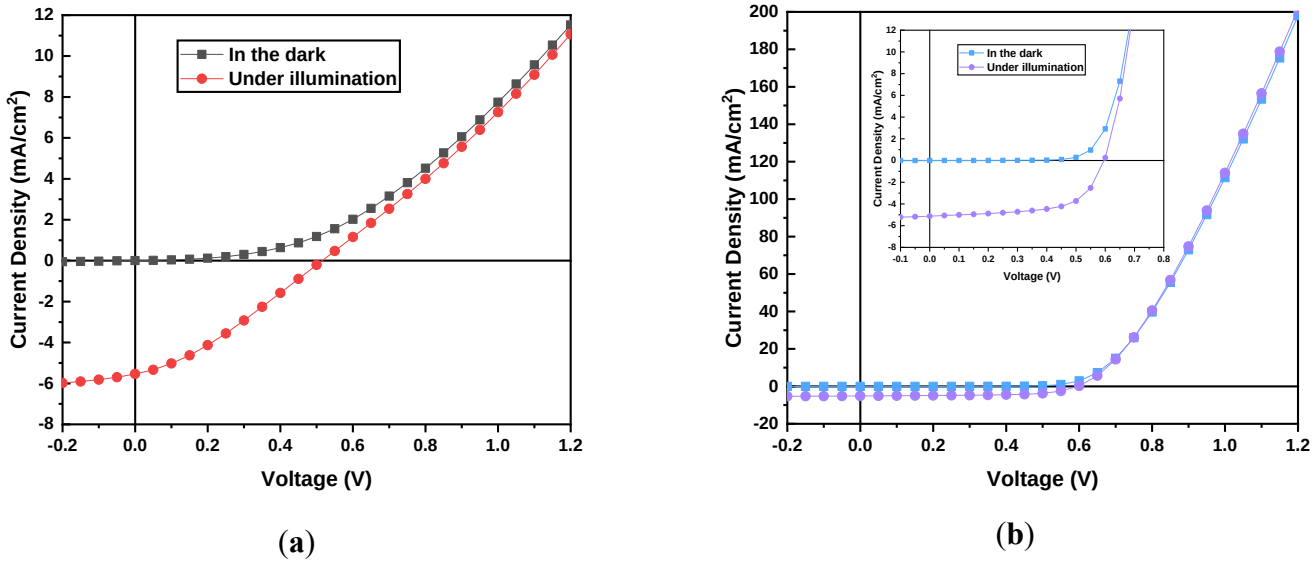

Figure 4. Photocurrent-Voltage (J-V) characteristics of (a) the SnO_2 based photovoltaic device and, (b) the ITO based photovoltaic device.

The SnO_2 based device has an open circuit voltage (V_{OC}) of 572 mV, a short circuit current density (J_{SC}) of 4.53 mA/cm^2, a fill factor (*FF*) of 30.7%, and a power conversion efficiency (*PCE*) of 0.79%. The obtained J_{SC} and V_{OC} are comparable to those the ITO based device, as opposed to the *FF* and *PCE* which are lower as shown in Table 3. This difference can be explained by the impact of the series (R_S) and the shunt (R_{Sh}) resistances, and by the electrical properties of both TCOs. The SnO_2 device presents an R_{Sh} of 3.97×10^3 Ω.cm^2 compared to 4.86×10^4 Ω.cm^2 for the ITO based device indicating the presence of greater number of shunt paths in the SnO_2 based

device compared to the ITO one. The higher dislocation density δ of the SnO_2 film, compared to the commercial ITO ($79.5 \pm 0.48\ 10^2$ lines/μm^2 for SnO_2 compared to $5.51 \pm 0.33\ 10^2$ lines/μm^2 for ITO), correlates with the assessment of made in regard of the shunt resistance. In addition, the SnO_2 based device presents a R_S of 187.3 Ω.cm^2 about ten times higher than for the ITO based device (17.3 Ω.cm^2). The main effect of such a high R_S is to reduce the *FF* as observed. Therefore, a lower *PCE* for the SnO_2 based device compared to the ITO based device is observed and could be attributed to the lower electrical properties for SnO_2 compared to ITO and therefore to the lower factor of merit Φ_{TC}. Nonetheless the SnO_2 based device is functional with a high V_{OC}. And to our knowledge no undoped SnO_2 was employed as electrode in OSCs, since most of research studies on SnO_2 thin films as TCOs are focused on foreign element doping[10,44]. These results are promising, since there is a hope to continue improving the electrical properties of SnO_2 films in order to reach efficiency close to the values obtained with ITO.

Table 3. Photovoltaic characteristics of the SnO_2 and ITO based photovoltaic devices.

Substrate	V_{OC} (mV)	J_{SC} (mA/cm²)	P_m (mW)	Fill Factor (%)	*PCE* (%)	R_S (Ω.cm^2)	R_{Sh} (Ω.cm^2)
SnO_2	572	5.98	7.959×10^{-5}	30.7	0.79	187.3	3.97×10^{3}
ITO	597	5.1	2.293×10^{-4}	61.5	1.91	17.3	4.86×10^{4}

4. CONCLUSION

Nanostructured SnO_2 films were deposited by (RF)-magnetron sputtering at different substrate temperatures for an Ar/O_2 gas flow ratio of 8/3. The structural, optical, and electrical properties of the films were investigated. The XRD profiles show that all deposited films are polycrystalline

and in the cassiterite tetragonal structure. The crystallinity of the films increases with the substrate temperature. The average transmittance of all the films is above 80% in the visible range and the optical band gap is around 4.0 eV. The SnO_2 film prepared at 100°C presents the lowest resistivity of 4.45×10^{-3} Ω.cm with a carrier concentration of 6.78×10^{19} cm^{-3}. The transmittance, optical bandgap, and work function SnO_2 films are similar to those of the commercial ITO. This leads to a figure of merit (Haacke) in the same range for both SnO_2 and ITO. The SnO_2 based device presents a J_{SC} and a V_{OC} values close to those obtained with the ITO based device, which is very promising. Indeed, the *PCE* of the OSC is lower for SnO_2 than ITO only because the fill factor is lower. Therefore, it is still possible to continue improving the electrical properties of the SnO_2 films by improving the surface quality (to raise the shunt resistance) and the conductivity (to lower the series resistance, possibly by adding dopants in SnO_2).The fact that the energy levels of ITO and SnO_2 are similar (bandgap, work function) demonstrates the potential of SnO_2 to replace ITO in organic solar cells.

Supplementary information

The supplementary information is available free of charge. It contains additional experimental details on the effect of O_2 partial pressure on the electrical properties of the elaborated SnO_2 thin films by (RF)-magnetron sputtering, for a fixed substrate temperature of 100°C.

The supplementary information also contains a description of the method of patterning the elaborated SnO_2 thin films.

Corresponding Author

* Email: wissal.belayachi@ipcms.unistra.fr.

Author Contributions

The manuscript was written through contributions of all authors. All authors have given approval to the final version of the manuscript.

Conceptualization, Gérald Ferblantier and Aziz Dinia; Formal analysis, Wissal Belayachi; Funding acquisition, Abdelilah Slaoui, Mohammed Abd-Lefdil and Aziz Dinia; Investigation, Wissal Belayachi, Thomas Fix, Stéphane Rocques, and Cédric Leuvrey; Methodology, Gérald Ferblantier, Stéphane Rocques, Nicolas Zimmermann, Cédric Leuvrey, Thomas Fix and Guy Schmerber; Project administration, Mohammed Abd-Lefdil and Aziz Dinia; Resources, Gérald Ferblantier, Guy Schmerber, Thomas Fix, Abdelilah Slaoui, Mohammed Abd-Lefdil and Aziz Dinia; Supervision, Gérald Ferblantier, Guy Schmerber, Abdelilah Slaoui, Mohammed Abd-Lefdil and Aziz Dinia; Validation, Gérald Ferblantier, Jean-Luc Rehspringer, Mohammed Abd-Lefdil and Aziz Dinia; Visualization, Wissal Belayachi; Writing – original draft, Wissal Belayachi;

Writing – review & editing, Wissal Belayachi, Gérald Ferblantier, Thomas Fix, Guy Schmerber, Jean-Luc Rehspringer, Thomas Heiser, Abdelilah Slaoui, Mohammed Abd-Lefdil and Aziz Dinia.

Funding Sources: This research was co-funded by H2020-MSCA-RISE-777968 and the Erasmus+ Program of the European Union, grant number 573722.

Acknowledgments: The authors thank the C3Fab platform (ICUBE. Strasbourg) for TCO thin films and solar cells characterizations, especially Nicolas Zimmerman for the patterning of SnO_2 films and preparation of the solar cells. The authors thank the SEM platform of CNRS-Cronenbourg, especially Cedric Leuvrey for the SEM and EDX observations, the DRX platform (IPCMS, Strasbourg), especially Marc Lenertz for the DRX observation. W.B. thanks the H2020 Marie Skłodowska-Curie Actions program and the Erasmus+ Program of the European Union project for financial support.

REFERENCES

(1) Granqvist, C. G. Transparent Conductors as Solar Energy Materials: A Panoramic Review. *Solar Energy Materials and Solar Cells* **2007**, *91* (17), 1529–1598. https://doi.org/10.1016/j.solmat.2007.04.031.

(2) Minami, T. Transparent Conducting Oxide Semiconductors for Transparent Electrodes. *Semicond. Sci. Technol.* **2005**, *20* (4), S35–S44. https://doi.org/10.1088/0268-1242/20/4/004.

(3) Kim, E.; Kwon, J.; Kim, C.; Kim, T.-S.; Choi, K. C.; Yoo, S. Design of Ultrathin OLEDs Having Oxide-Based Transparent Electrodes and Encapsulation with Sub-Mm Bending Radius. *Organic Electronics* **2020**, *82*, 105704. https://doi.org/10.1016/j.orgel.2020.105704.

(4) Template Deformation-Tailored ZnO Nanorod/Nanowire Arrays: Full Growth Control and Optimization of Field-Emission - Zeng - 2009 - Advanced Functional Materials - Wiley Online Library https://onlinelibrary.wiley.com/doi/10.1002/adfm.200900714 (accessed 2021 -08 -28).

(5) Chen, Z.; Pan, D.; Li, Z.; Jiao, Z.; Wu, M.; Shek, C.-H.; Wu, C. M. L.; Lai, J. K. L. Recent Advances in Tin Dioxide Materials: Some Developments in Thin Films, Nanowires, and Nanorods. *Chem. Rev.* **2014**, *114* (15), 7442–7486. https://doi.org/10.1021/cr4007335.

(6) Fortunato, E.; Ginley, D.; Hosono, H.; Paine, D. C. Transparent Conducting Oxides for Photovoltaics. *MRS Bulletin* **2007**, *32* (3), 242–247. https://doi.org/10.1557/mrs2007.29.

(7) Ihokura, K.; Watson, J. *The Stannic Oxide Gas Sensor: Principles and Applications*; CRC Press: Boca Raton, 2020. https://doi.org/10.1201/9780203735893.

(8) Lalauze, R.; Breuil, P.; Pijolat, C. Thin Films for Gas Sensors. *Sensors and Actuators B: Chemical* **1991**, *3* (3), 175–182. https://doi.org/10.1016/0925-4005(91)80003-3.

(9) Batzill, M.; Diebold, U. The Surface and Materials Science of Tin Oxide. *Progress in Surface Science* **2005**, *79* (2), 47–154. https://doi.org/10.1016/j.progsurf.2005.09.002.

(10) Yang, W.; Yu, S.; Zhang, Y.; Zhang, W. Properties of Sb-Doped SnO2 Transparent Conductive Thin Films Deposited by Radio-Frequency Magnetron Sputtering. *Thin Solid Films* **2013**, *542*, 285–288. https://doi.org/10.1016/j.tsf.2013.06.077.

(11) Bansal, S.; Pandya, D. K.; Kashyap, S. C. Charge Transport Mechanism in High Conductivity Undoped Tin Oxide Thin Films Deposited by Reactive Sputtering. *Thin Solid Films* **2012**, *524*, 30–34. https://doi.org/10.1016/j.tsf.2012.09.062.

(12) Wang, Y.; Ma, J.; Ji, F.; Yu, X.; Ma, H. Structural and Photoluminescence Characters of SnO2:Sb Films Deposited by RF Magnetron Sputtering. *Journal of Luminescence* **2005**, *114* (1), 71–76. https://doi.org/10.1016/j.jlumin.2004.12.003.

(13) Montero, J.; Guillén, C.; Herrero, J. Nanocrystalline Antimony Doped Tin Oxide (ATO) Thin Films: A Thermal Restructuring Study. *Surface and Coatings Technology* **2012**, *211*, 37–40. https://doi.org/10.1016/j.surfcoat.2011.07.068.

(14) Ferreira, M.; Loureiro, J.; Nogueira, A.; Rodrigues, A.; Martins, R.; Ferreira, I. SnO2 Thin Film Oxides Produced by Rf Sputtering for Transparent Thermoelectric Devices. *Materials Today: Proceedings* **2015**, *2* (2), 647–653. https://doi.org/10.1016/j.matpr.2015.05.090.
(15) Kaur, M.; Dadhich, B. K.; Singh, R.; KailasaGanapathi; Bagwaiya, T.; Bhattacharya, S.; Debnath, A. K.; Muthe, K. P.; Gadkari, S. C. RF Sputtered SnO2: NiO Thin Films as Sub-Ppm H2S Sensor Operable at Room Temperature. *Sensors and Actuators B: Chemical* **2017**, *242*, 389–403. https://doi.org/10.1016/j.snb.2016.11.054.
(16) Ma, J.; Hao, X.; Ma, H.; Xu, X.; Yang, Y.; Huang, S.; Zhang, D.; Cheng, C. RF Magnetron Sputtering SnO2: Sb Films Deposited on Organic Substrates. *Solid State Communications* **2002**, *121* (6), 345–349. https://doi.org/10.1016/S0038-1098(02)00009-1.
(17) de Moure-Flores, F.; Quiñones-Galván, J. G.; Hernández-Hernández, A.; Guillén-Cervantes, A.; Santana-Aranda, M. A.; Olvera, M. de la L.; Meléndez-Lira, M. Structural, Optical and Electrical Properties of Cd-Doped SnO2 Thin Films Grown by RF Reactive Magnetron Co-Sputtering. *Applied Surface Science* **2012**, *258* (7), 2459–2463. https://doi.org/10.1016/j.apsusc.2011.10.072.
(18) Xu, B.; Ren, X.-G.; Gu, G.-R.; Lan, L.-L.; Wu, B.-J. Structural and Optical Properties of Zn-Doped SnO2 Films Prepared by DC and RF Magnetron Co-Sputtering. *Superlattices and Microstructures* **2016**, *89*, 34–42. https://doi.org/10.1016/j.spmi.2015.10.043.
(19) Aragón, F. H.; Aquino, J. C. R.; Gomes, N. C. S.; Ardisson, J. D.; da Silva, S. W.; Pacheco-Salazar, D. G.; Coaquira, J. A. H. Characterization of Polycrystalline SnO2 Films Deposited by DC Sputtering Technique with Potential for Technological Applications. *Journal of the European Ceramic Society* **2017**, *37* (10), 3375–3380. https://doi.org/10.1016/j.jeurceramsoc.2017.04.014.
(20) Mehraj, S.; Ansari, M. S.; Alimuddin. Annealed SnO2 Thin Films: Structural, Electrical and Their Magnetic Properties. *Thin Solid Films* **2015**, *589*, 57–65. https://doi.org/10.1016/j.tsf.2015.04.065.
(21) Singh, J.; Kumar, R.; Verma, V.; Kumar, R. Structural and Optoelectronic Properties of Epitaxial Ni-Substituted Cr2O3 Thin Films for p-Type TCO Applications. *Materials Science in Semiconductor Processing* **2021**, *123*, 105483. https://doi.org/10.1016/j.mssp.2020.105483.
(22) Patel, P.; Karmakar, A.; Jariwala, C.; Ruparelia, J. P. Preparation and Characterization of SnO2 Thin Film Coating Using Rf-Plasma Enhanced Reactive Thermal Evaporation. *Procedia Engineering* **2013**, *51*, 473–479. https://doi.org/10.1016/j.proeng.2013.01.067.
(23) Yadav, S.; Kumari, S.; Ghoshal, S. K.; Kumar, R.; Chaudhary, S. K.; Mohan, D. Effect of Ultraviolet Radiation Exposure on Optical Nonlinearity and Switching Traits of SnO2 Thin Films Deposited by Thermal Evaporation. *Optics & Laser Technology* **2021**, *133*, 106575. https://doi.org/10.1016/j.optlastec.2020.106575.
(24) Vaufrey, D.; Ben Khalifa, M.; Besland, M. P.; Sandu, C.; Blanchin, M. G.; Teodorescu, V.; Roger, J. A.; Tardy, J. Reactive Ion Etching of Sol–Gel-Processed SnO2 Transparent

Conducting Oxide as a New Material for Organic Light Emitting Diodes. *Synthetic Metals* **2002**, *127* (1), 207–211. https://doi.org/10.1016/S0379-6779(01)00624-5.
(25) Seo, M.; Akutsu, Y.; Kagemoto, H. Preparation and Properties of Sb-Doped SnO2/Metal Substrates by Sol–Gel and Dip Coating. *Ceramics International* **2007**, *33* (4), 625–629. https://doi.org/10.1016/j.ceramint.2005.11.013.
(26) Carvalho, D. H. Q.; Schiavon, M. A.; Raposo, M. T.; de Paiva, R.; Alves, J. L. A.; Paniago, Roberto. M.; Speziali, N. L.; Ferlauto, A. S.; Ardisson, J. D. Synthesis and Characterization of SnO2 Thin Films Prepared by Dip-Coating Method. *Physics Procedia* **2012**, *28*, 22–27. https://doi.org/10.1016/j.phpro.2012.03.664.
(27) Bouznit, Y.; Henni, A. Characterization of Sb Doped SnO2 Films Prepared by Spray Technique and Their Application to Photocurrent Generation. *Materials Chemistry and Physics* **2019**, *233*, 242–248. https://doi.org/10.1016/j.matchemphys.2019.05.072.
(28) Korotcenkov, G.; Brinzari, V.; Boris, Y.; Ivanov, M.; Schwank, J.; Morante, J. Influence of Surface Pd Doping on Gas Sensing Characteristics of SnO2 Thin Films Deposited by Spray Pirolysis. *Thin Solid Films* **2003**, *436* (1), 119–126. https://doi.org/10.1016/S0040-6090(03)00506-6.
(29) Dagkaldiran, Ü.; Gordijn, A.; Finger, F.; Yates, H. M.; Evans, P.; Sheel, D. W.; Remes, Z.; Vanecek, M. Amorphous Silicon Solar Cells Made with SnO2:F TCO Films Deposited by Atmospheric Pressure CVD. *Materials Science and Engineering: B* **2009**, *159–160*, 6–9. https://doi.org/10.1016/j.mseb.2008.10.037.
(30) Sharma, S.; Chhoker, S. CVD Grown Doped and Co-Doped SnO2 Nanowires and Its Optical and Electrical Studies. *Materials Today: Proceedings* **2020**, *28*, 375–378. https://doi.org/10.1016/j.matpr.2020.02.774.
(31) Karunakaran, C.; Sakthi Raadha, S.; Gomathisankar, P. Microstructures and Optical, Electrical and Photocatalytic Properties of Sonochemically and Hydrothermally Synthesized SnO2 Nanoparticles. *Journal of Alloys and Compounds* **2013**, *549*, 269–275. https://doi.org/10.1016/j.jallcom.2012.09.035.
(32) Cao, X.; Shu, Y.; Hu, Y.; Li, G.; Liu, C. Integrated Process of Large-Scale and Size-Controlled SnO2 Nanoparticles by Hydrothermal Method. *Transactions of Nonferrous Metals Society of China* **2013**, *23* (3), 725–730. https://doi.org/10.1016/S1003-6326(13)62521-2.
(33) Kim, S. E.-K.; Oliver, M. Structural, Electrical, and Optical Properties of Reactively Sputtered SnO2 Thin Films. *Met. Mater. Int.* **2010**, *16* (3), 441–446. https://doi.org/10.1007/s12540-010-0614-6.
(34) Scherrer, P. Bestimmung Der Größe Und Der Inneren Struktur von Kolloidteilchen Mittels Röntgenstrahlen. **1918**.

(35) Uvarov, V.; Popov, I. Metrological Characterization of X-Ray Diffraction Methods at Different Acquisition Geometries for Determination of Crystallite Size in Nano-Scale Materials. *Materials Characterization* **2013**, *85*, 111–123. https://doi.org/10.1016/j.matchar.2013.09.002.
(36) Williamson, G. K.; Smallman, R. E. III. Dislocation Densities in Some Annealed and Cold-Worked Metals from Measurements on the X-Ray Debye-Scherrer Spectrum. *The Philosophical Magazine: A Journal of Theoretical Experimental and Applied Physics* **1956**, *1* (1), 34–46. https://doi.org/10.1080/14786435608238074.
(37) Gorley, P. M.; Khomyak, V. V.; Bilichuk, S. V.; Orletsky, I. G.; Horley, P. P.; Grechko, V. O. SnO2 Films: Formation, Electrical and Optical Properties. *Materials Science and Engineering: B* **2005**, *118* (1), 160–163. https://doi.org/10.1016/j.mseb.2004.12.026.
(38) Alhuthali, A.; El-Nahass, M. M.; Atta, A. A.; Abd El-Raheem, M. M.; Elsabawy, K. M.; Hassanien, A. M. Study of Topological Morphology and Optical Properties of SnO2 Thin Films Deposited by RF Sputtering Technique. *Journal of Luminescence* **2015**, *158*, 165–171. https://doi.org/10.1016/j.jlumin.2014.09.044.
(39) Minami, T.; Nanto, H.; Takata, S. Highly Conducting and Transparent SnO2 Thin Films Prepared by RF Magnetron Sputtering on Low-Temperature Substrates. *Jpn. J. Appl. Phys.* **1988**, *27* (3A), L287. https://doi.org/10.1143/JJAP.27.L287.
(40) *Amorphous and Liquid Semiconductors*; Tauc, J., Ed.; Springer US, 1974. https://doi.org/10.1007/978-1-4615-8705-7.
(41) Kim, I. H.; Ko, J. H.; Kim, D.; Lee, K. S.; Lee, T. S.; Jeong, J. -h.; Cheong, B.; Baik, Y.-J.; Kim, W. M. Scattering Mechanism of Transparent Conducting Tin Oxide Films Prepared by Magnetron Sputtering. *Thin Solid Films* **2006**, *515* (4), 2475–2480. https://doi.org/10.1016/j.tsf.2006.07.020.
(42) Beensh-Marchwicka, G.; Król-Stępniewska, L.; Misiuk, A. High Temperature Oxidized SnO2 Films Prepared by Reactive Sputtering. *Active and Passive Electronic Components* **1987**, *12* (3), 191–200. https://doi.org/10.1155/1987/49720.
(43) Haacke, G. New Figure of Merit for Transparent Conductors. *Journal of Applied Physics* **2008**, *47* (9), 4086. https://doi.org/10.1063/1.323240.
(44) Lee, J.; Kim, N.-H.; Park, Y. S. Characteristics of SnO2:Sb Films as Transparent Conductive Electrodes of Flexible Inverted Organic Solar Cells. *Journal of Nanoscience and Nanotechnology* **2016**, *16* (5), 4973–4977. https://doi.org/10.1166/jnn.2016.12173.

Table of Content

List of tables